NATIONAL ADVISORY COMMITTEE FOR AERONAUTICS

TECHNICAL NOTE

No. 1330

EFFECT OF CRITICAL MACH NUMBER AND FLUTTER ON MAXIMUM POWER LOADING OF DUCTED FANS

By Arthur A. Regier, John G. Barmby, and Harvey H. Hubbard

Langley Memorial Aeronautical Laboratory
Langley Field, Va.

Washington

June 1947

NATIONAL ADVISORY COMMITTEE FOR AERONAUTICS

TECHNICAL NOTE NO. 1330

EFFECT OF CRITICAL MACH NUMBER AND FLUTTER ON MAXIMUM POWER LOADING OF DUCTED FANS

By Arthur A. Regier, John G. Barmby, and Harvey H. Hubbard

SUMMARY

Flutter tests were made of two wind-tunnel-fan models, one of which had conventional Clark Y airfoil sections and the other of which had high-camber blade sections. The results of the tests confirm the stall-flutter theory which predicts much higher flutter speeds at the high lift coefficients for the high-camber blades. The high-camber blades could, therefore, be operated at much higher power loading than could the low-camber blades. Aerodynamic data of these tests indicated little difference in efficiency for the two fans but somewhat higher maximum lift coefficient for the high-camber fan. The efficiency of the fans decreased after the velocity, as calculated by two-dimensional theory, exceeded the speed of sound on the upper blade surface.

An analysis is made of the factors that determine the power loading of a fan blade section. Graphs are presented which give the maximum power loading for idealized sections of various thickness ratios operating at the critical Mach number.

Examples show that the ideal or design lift coefficient of an airfoil is almost the same as the lift coefficient giving the maximum flutter speed. It is therefore desirable that a section be operated at the ideal lift in order to obtain high critical speeds as well as the maximum margin of safety with respect to flutter.

INTRODUCTION

An important problem in the design of ducted fans, such as wind-tunnel fans and axial compressors, is the absorption of maximum power at high efficiency without blade failure. The present paper is concerned with two of the factors which may limit the power loading of fans. These factors are the flutter speed and the critical Mach number of the blade section.

The flutter speed is shown in reference 1 to depend on the lift coefficient of the blade. For operation at high lift coefficients, theory shows that the flutter speed can be increased by properly cambering the blade section. In order to check this theory, a model fan having high-camber blades was built and tested and the results were compared with those for a fan having Clark Y airfoil sections. The results of these tests are reported in the present paper.

In order to determine to what extent high lift coefficients can be used to advantage, an analysis is made in which the critical Mach numbers of the blade sections are taken into consideration. Relations for the power loading and the pressure rise are obtained, and the maximum power loading per unit blade area is given for idealized airfoil sections of different thickness ratios operating at the critical Mach number. The analysis applies only to a blade element operating at ideal conditions and, therefore, cannot be directly applied to the performance of the entire blade. The analysis serves, however, to show the important parameters and gives an upper limit to the useful power that can be absorbed if the section critical Mach number is considered to correspond to the limiting speed for efficient operation.

SYMBOLS

T	thrust, pounds
V	axial velocity of stream, feet per second
ρ	density, slugs per cubic foot
W	resultant velocity at blade section, feet per second
c	chord, feet
A	blade area, square feet
M	Mach number
M_t	helical tip Mach number
a	speed of sound in air, feet per second
P	power, foot pounds per second
P_A	power loading per unit blade area, horsepower per square foot

C_L	lift coefficient
ϕ	geometric helix angle, degrees
r	radius to propeller section, feet
R	propeller tip radius, feet
B	number of blades
σ	solidity
C_p	pressure coefficient
$\frac{dC_L}{d\alpha}$	slope of lift curve
$C_{m_{c/4}}$	pitching-moment coefficient about quarter-chord point
x	distance along x-axis, chords
y	distance along y-axis, chords
$x_{c.g.}$	location of center of gravity as measured from leading edge, chords
$C_{L_{u_I}}$	lift coefficient for ideal no-twist condition
C_{L_u}	untwisted or design value of lift coefficient
q	dynamic pressure of operating speed, pounds per square foot $\left(\frac{1}{2}\rho W^2\right)$
K	torsional stiffness of blade, foot-pound per radian
G	shear modulus of elasticity, pounds per square foot
J	torsion modulus of section, $feet^4$
t	thickness of section, feet
L	representative length of blade, feet
Q	quantity rate of flow through fan, cubic feet per second
Δp	pressure rise through fan, pounds per square foot
$M_{f_{cal}}$	calculated classical-flutter tip Mach number

$M_{f_{max}}$ maximum measured flutter tip Mach number

$M_{f_{min}}$ minimum measured stall-flutter tip Mach number

α section angle of attack, degrees

β blade angle at radius r, degrees

Ω angular velocity of propeller, radians per second

η efficiency

a' rotational-velocity interference factor

Subscripts:

u untwisted or design

cr critical

I ideal

div divergence speed

f flutter speed

i incompressible

M conditions at critical Mach number

max maximum

0 standard conditions

THEORETICAL ANALYSIS

Relations for Power Loading and Pressure Rise

The following analysis is based on simple blade-element theory and neglects the drag forces and the change of density of the fluid passing through the fan. The quantities considered are shown in figure 1. The useful power is given by the product of the thrust T and the axial velocity V.

For an element of blade radius dr the relations for the power are as follows:

$$dP = V\,dT = V\,dL\cos\phi$$

where

$$dL = \frac{1}{2}\rho W^2 C_L c\,dr$$

$$V = W\sin\phi$$

Therefore,

$$dP = \frac{1}{2}\rho W^3 C_L \cos\phi \sin\phi\, c\,dr$$

Since

$$c\,dr = dA$$

and

$$\cos\phi \sin\phi = \frac{1}{2}\sin 2\phi$$

$$\frac{dP}{dA} = \frac{1}{4}\rho W^3 C_L \sin 2\phi \qquad (1)$$

The quantity dP/dA is the power loading per unit blade area. When the resultant blade-element velocity W is expressed in terms of Mach number M and speed of sound a, equation (1) may be written

$$\frac{dP}{dA} = \frac{1}{4}\rho C_L M^3 a^3 \sin 2\phi \qquad (2)$$

If the geometric helix angle ϕ is 45°, the power loading per unit blade area is a maximum; that is,

$$\left(\frac{dP}{dA}\right)_{max} = \frac{1}{4}\rho C_L M^3 a^3 \tag{3}$$

A convenient expression for the maximum power loading per unit blade area $P_{A_{max}}$ expressed in horsepower per square foot for air at standard conditions is

$$P_{A_{max}} = \frac{1}{4}\left(\frac{0.002378 \times 1116^3}{550}\right) C_L M^3$$

$$= 1500\ C_L M^3 \tag{4}$$

Equation (4) may be written in a more general form for any density and speed of sound as

$$P_{A_{max}} = 1500\ \frac{\rho}{\rho_0}\left(\frac{a}{a_0}\right)^3 C_L M^3 \tag{5}$$

where ρ_0 refers to density of air at standard conditions and a_0, to speed of sound in air at standard conditions.

An expression for the pressure rise may be obtained by equating the thrust of the fan blade elements to the product of the pressure rise Δp times the area through which the blade elements sweep. Thus, for a fan having a given number of blades B and a blade-element radius dr

$$B\ dT = \Delta p 2\pi r\ dr$$

$$\Delta p = \frac{B\ dT}{2\pi r\ dr}$$

$$= \frac{\frac{1}{2}\rho w^2 C_L B c\ dr \cos \phi}{2\pi r\ dr}$$

Since

$$\frac{Bc}{2\pi r} = \sigma$$

$$\Delta p = \frac{1}{2}\rho W^2 C_L \sigma \cos \phi \tag{6}$$

Or, in terms of M and a,

$$\Delta p = \frac{1}{2}\rho C_L M^2 a^2 \sigma \cos \phi \tag{7}$$

It may be noted that the maximum value of Δp occurs when ϕ is 0°; whereas the maximum value of P_A occurs when ϕ is 45°.

Maximum Power Loading as Limited by Critical Mach Number

Equation (3) shows that the power loading is proportional to $C_L M^3$. Increasing the lift coefficient generally decreases the critical Mach number. The problem is therefore to find the value of C_{L_M} and the associated section critical Mach number M_{cr} such that the product of $C_{L_M} M_{cr}^3$ is a maximum. In the present analysis the critical Mach number of the blade section is assumed to be the upper limit of efficient operation.

Idealized sections.– Max. A. Heaslet of the Ames Aeronautical Laboratory of the NACA has shown the relation between critical Mach number and lift coefficient for various airfoils. As a limiting case an idealized section with elliptical thickness distribution was used; this section carried lift with a flat-top lift distribution in which one-half of the lift was considered to act on the lower surface and one-half, on the upper surface. Such an idealized section has been used in the present paper to evaluate the quantity $C_{L_M} M_{cr}^3$ for various thickness ratios.

The method used for calculating the critical speed of an airfoil at a given lift coefficient consists of first calculating the potential two-dimensional pressure distribution. (See references 2 to 4.) The peak negative pressure is then corrected for compressibility, and the stream Mach number is found at which the local Mach number is unity. The lift coefficient for incompressible flow is then corrected for compressibility to this stream Mach number. This lift coefficient is designated C_{l_M} and the corresponding stream Mach number is designated M_{cr}. For simplicity and consistency both the peak pressure coefficient and the lift coefficient have been corrected in the present paper by means of the Prandtl-Glauert factor as follows:

$$C_{l_M} = \frac{C_{l_i}}{\sqrt{1 - M_{cr}^2}}$$

and

$$C_{p_M} = \frac{C_{p_i}}{\sqrt{1 - M_{cr}^2}}$$

In figure 2 the values of $C_{l_M} M_{cr}^3$ and maximum power loading $P_{A_{max}}$ (hp/sq ft) are plotted against C_{l_M} for the family of hypothetical idealized airfoil sections. Lines of constant critical Mach number are also shown. The figure shows that for these idealized airfoil sections, the power loading becomes greater for the higher lift coefficients. For example, a 9-percent-thick airfoil section operating at $C_{l_M} = 0.3$ has a critical Mach number of 0.8 and a power loading of 225 horsepower per square foot. A section of the same thickness operating at $C_{l_M} = 1.05$ has a critical Mach number of 0.7 and a power loading of 540 horsepower per square foot. The maximum power loading occurs at the highest lift coefficient at which the section operates. If the curves were extended far enough, they would have maximum values of $C_{l_M} M_{cr}^3$, but the curves were calculated only to a value of 1.6 for C_{l_M} since this value already is higher than that normally obtained in practice.

Figure 2 also shows the advantage of using thin airfoil sections to absorb higher power. The power loading at $C_{l_M} = 0.8$ is 516 horse-

power per square foot for a 6-percent-thick airfoil section and 390 horsepower per square foot for a 15-percent-thick airfoil section. This conclusion regarding the effect of thickness applies only for airfoils operating at the design lift coefficient. Because of high peak pressures at other than the design lift coefficient, the thin airfoil sections may not have the advantage shown by figure 2.

Conventional airfoil sections.- As pointed out by Heaslet the idealized sections are not practical airfoils, chiefly because the elliptical thickness distribution would cause flow separation on the afterbody; thus, high drag would result. The idealized section of a given thickness ratio, furthermore, represents a different shape airfoil for each lift coefficient. Thus, the curves in figure 2 for 6-percent thickness represent not one airfoil shape but an infinite number of airfoil shapes of 6-percent thickness. In order to determine how near conventional airfoils approach the idealized section in critical Mach number and power loading, three conventional airfoils are compared with the idealized sections of the same thickness.

The three conventional airfoils are a Clark Y airfoil section having 11.7-percent thickness and 3.5-percent camber, a Clark YM airfoil section with the same thickness distribution but with 9-percent camber, and an NACA 16-series airfoil of 12-percent thickness, 5.5-percent camber, and a design lift of 1.0. The airfoil shapes are shown in figure 3. The coordinates of the first and second airfoils are given in reference 3 and the coordinates of the last airfoil are in reference 4.

The critical Mach number as determined theoretically is plotted in figure 4 for the conventional airfoils and the 12-percent-thick idealized airfoil. The critical Mach number for the idealized-airfoil curve decreases with an increase in lift coefficient. Each conventional airfoil is seen to approach the curve of the idealized airfoil over a certain range of C_{l_M}. This favorable range coincides approximately with the design or ideal lift of the particular airfoil. At low values of the lift coefficient the critical Mach numbers may be low because of the high velocity at the front lower surface of the airfoil.

Figure 5 gives the maximum power loading for the same airfoils. The power loadings for the high-camber airfoils become favorable only at the higher lift coefficients. At the high lift coefficients

the high-camber sections have higher power loadings than the low-camber section. Some doubt exists, however, as to the maximum lift coefficient that can be used in practice without separation of flow resulting in low efficiency.

The design of the whole blade for a given operating condition is beyond the scope of the present paper. If the entire area of a propeller or fan blade is considered, the average power loading is much lower than the maximum power loading which refers only to the loading of an isolated blade section operating at its critical speed. This difference occurs because the inboard sections are operating at much lower stream Mach numbers and because the helix angle varies along the blade. The average power loading is probably increased by reducing the tip lift coefficient and increasing the tip Mach number; thereby, the power loading of the inboard sections is increased.

Maximum Power Loading as Limited by Flutter Speed

Flutter is a self-excited oscillation of a body caused by energy absorbed from the air stream. This oscillation is usually very violent and destructive. The two principal types of flutter are classical flutter and stall flutter. Classical flutter is an oscillatory instability of an airfoil operating in a potential flow. In general, such flutter requires at least two coupled degrees of freedom, such as bending and torsion. Stall flutter is caused by separation of flow and occurs on airfoils operating near or in the stall condition of flow. This type of flutter requires only one degree of freedom, usually torsion, and is generally attributed to the hysteresis in the lift curve near stall.

In reference 1 the classical flutter speed and the divergence speed are shown to be almost the same for propellers and fans. A design sufficiently rigid to preclude divergence is usually safe against classical flutter. The aerodynamic moment may however appreciably twist the blade at much lower speeds. This twisting may change the angle of attack sufficiently to cause stall flutter.

In reference 1 the stall flutter was seen to occur on a conventional Clark Y airfoil section when the blade twisted sufficiently to increase the lift coefficient to about $C_L = 1.0$. This value cannot be taken as an absolute limit since the stall characteristic depends on Reynolds number, Mach number, and type of airfoil. No aerodynamic twisting moment would be present on the blade if the aerodynamic center of pressure of the blade section coincided with the center of gravity of the section (reference 1). For this condition the blade does not twist until the divergence speed is reached. The relation for this lift coefficient of no twist is given in reference 1 as

$$C_{L_{u_I}} = -\frac{C_{m_{c/4}}}{x_{c.g.} - \frac{1}{4}} \tag{8}$$

where

$C_{m_{c/4}}$ pitching-moment coefficient about quarter-chord point

$x_{c.g.}$ location of center of gravity as measured from leading edge, chords

If the lift coefficient is greater than $C_{L_{u_I}}$, the airfoil flutters at reduced speed with positive stall; if the lift coefficient is less than $C_{L_{u_I}}$, flutter occurs at reduced speed with negative stall. In either case, the maximum power that the blade absorbs occurs when the blade is operating at its lift coefficient of no twist $C_{L_{u_I}}$.

The following equations, based on equations from reference 1, have been used to calculate the lift coefficient at flutter speed for any value of C_{L_u}:

$$C_L = C_{L_u}\left(\frac{1}{1 - \frac{q}{q_{div}}}\right) - C_{L_{u_I}}\left(\frac{q/q_{div}}{1 - \frac{q}{q_{div}}}\right) \tag{9}$$

and

$$C_{L_u} = C_L - \frac{q}{q_{div}}\left(C_L - C_{L_{u_I}}\right) \tag{10}$$

where

C_L lift coefficient

C_{L_u} untwisted or design value of lift coefficient

$C_{L_{u_I}}$ lift coefficient for ideal no-twist condition

q/q_{div} dynamic pressure of operating speed divided by dynamic pressure of divergence speed

From equation (1) the power loading is seen to be proportional to W^3C_L. Since q is proportional to W^2, the power loading for a given value of q_{div} is therefore proportional to $C_L\left(\frac{q}{q_{div}}\right)^{3/2}$. Figure 6(a) gives the relative maximum power loading at flutter speed for the condition that C_{L_u} is greater than $C_{L_{u_I}}$. The curves are calculated by use of equation (10) on the assumption that flutter occurs when $C_L = 1.0$. As was pointed out previously, all airfoils do not flutter at exactly $C_L = 1.0$. The use in this analysis of this value for C_L as the lift coefficient at which flutter occurs is for purposes of estimating the variation of power loading for various values of C_{L_u} and $C_{L_{u_I}}$.

If C_{L_u} is less than $C_{L_{u_I}}$, the operating lift coefficient decreases with increased speed and the maximum power loading drops off very rapidly as C_{L_u} differs from $C_{L_{u_I}}$. In this case the maximum power does not occur at the flutter speed but at some point below the flutter speed. The maximum power loading for various values of $C_{L_{u_I}}$ is plotted in figure 6(b). The curves in this figure were obtained by graphical methods and use of equation (9).

Figure 6(a) shows that if a blade section having a value of $C_{L_{u_I}} = 0.4$ is operated at $C_{L_u} = 0.8$ the blade absorbs only 0.2 of the power it would absorb if it were operated at $C_{L_u} = 0.4$. Figure 6(b) shows that if the blade section having a value of $C_{L_{u_I}} = 0.4$ were operated at $C_{L_u} = 0.2$ the blade absorbs only 0.02 of the power it absorbs when operated at $C_{L_u} = 0.4$. This example illustrates that for a blade to absorb maximum power, C_{L_u} should equal $C_{L_{u_I}}$; and, if a deviation exists, the value of C_{L_u} should be greater than $C_{L_{u_I}}$ rather than smaller. These conditions are in line with standard practice.

The dynamic pressure of divergence speed q_{div} is that pressure at which the aerodynamic-moment stiffness of the blade equals the torsional stiffness at the blade and may be obtained from vibration data as indicated in references 1 and 5. Reference 1 gives an expression for the divergence speed in terms of the torsional stiffness of the blade as follows:

$$q_{div} = \frac{K}{Lc^2 \frac{dC_L}{d\alpha}\left(x_{c.g.} - \frac{1}{4}\right)} \tag{11}$$

where

L representative length of blade, feet

c chord, feet

$x_{c.g.}$ location of center of gravity as measured from leading edge, chords

K torsional stiffness of blade, foot-pound per radian

The torsional stiffness K is proportional to $\frac{GJ}{L}$ where G is the shear modulus of elasticity of the material and J is the torsion modulus of the section. For thin sections, J is approximately proportional to t^3c where t is the thickness of the section. Equation (11) may be written

$$q_{div} \propto \frac{G\left(\frac{t}{c}\right)^3 c^2}{\left(x_{c.g.} - \frac{1}{4}\right)\frac{dC_L}{d\alpha} L^2} \tag{12}$$

Equation (12) shows that q_{div} varies directly as the shear modulus of the material, as the cube of the thickness ratio, and as the square of the chord-length ratio and varies inversely as the distance of the section center of gravity from the quarter-chord position. For example, if the blade thickness is increased from 6 percent to 15 percent, q_{div} is increased by a factor of $\left(\frac{15}{6}\right)^3$ or 15.6. If a blade is made with a sufficiently large thickness ratio or sufficiently large chord-length ratio, the flutter problem can be eliminated entirely. This increase of ratios, however, is done at the expense of more weight or of poor aerodynamic characteristics and lower critical speeds.

The stall-flutter speed expressed in terms of dynamic pressure may be obtained from equation (10) on the assumption that flutter occurs at a given lift coefficient C_L. The equation is

$$q_f = q_{div}\left(\frac{C_{L_f} - C_{L_u}}{C_{L_f} - C_{L_{u_I}}}\right) \tag{13}$$

For positive stall flutter, $C_{L_f} > C_{L_u} > C_{L_{u_I}}$. If C_{L_u} equals $C_{L_{u_I}}$, the term in the parentheses equals unity, which is its maximum value. Any deviation from this condition reduced the flutter speed. By proper design of the chordwise load distribution, $C_{L_{u_I}}$ may be made identical to the ideal or design lift coefficient of the blade section. The ideal lift corresponds to the lift at the ideal angle of attack, which is defined as the angle at which the front stagnation point is at the leading edge of the airfoil. If the section is operated at this ideal lift, the highest critical speed and best flow conditions are obtained for that operating condition. (See reference 6.)

For the homogeneous conventional airfoil sections considered in the present paper, C_{L_I} is almost equal to $C_{L_{u_I}}$. Table I gives the values of $C_{L_{u_I}}$ and C_{L_I} for the three airfoil sections previously discussed. The values of $C_{L_{u_I}}$ are calculated by equation (8). The values of $C_{m_{c/4}}$ and C_{L_I} were obtained from potential calculations. As seen from table I, operating the airfoils at $C_{L_{u_I}}$ has no disadvantages since C_{L_I} and $C_{L_{u_I}}$ are almost the same.

The value of q_{div} that should be used depends on the application. In general, a very high value of q_{div} gives a stiffer blade having a longer operating life, particularly in applications where vibration is severe. A high value of q_{div} is also necessary where the operating conditions vary widely, that is, where the value of C_{L_u} varies over wide limits. Equation (13) shows that for such conditions q_f may be only a small fraction of q_{div}. In some wind-tunnel fans and axial-flow compressors, however, the operating condition with respect to the blade lift coefficients does not vary appreciably. In such cases a lighter blade having a lower value of q_{div} may be successfully used. It appears that the most economical and efficient design would be one

in which $C_{L_{u_I}}$ of the blade were equal to the minimum operating lift coefficient for maximum speed. In general, such a design gives the highest critical speed as well as the greatest flutter safety margin for a given value of q_{div}.

EXPERIMENTAL STUDIES OF FAN FLUTTER AT HIGH LOADING

Equipment and Test Procedure

Wind-tunnel-fan models were tested in the same open-return tunnel used for the tests of reference 1. A diagramatic sketch of the test setup is shown in figure 7. The blade tips were illuminated by stroboscopic light and observed in operation by means of a window in the tunnel wall. The blade load and C_{L_u} of the blade were varied by means of slats in the tunnel exit. These slats change the tunnel velocity and thereby change the angle of attack of the fan blades.

The fans are made of laminated Sitka spruce and have a specific gravity of about 0.5 and a diameter of 45 inches. Blade-form curves for the fans tested are shown in figure 8. The fans are as follows:

Fan A is a six-blade fan having conventional Clark Y airfoil sections. This fan is the same as the fan designated in reference 1 as propeller A.

Fan B is a four-blade fan having Clark YM airfoil sections of 9-percent camber. This fan has the same blade dimensions and lift distribution along the blade as fan A. Fan B is also operated as a six-blade fan to obtain some flutter points at low lift coefficients. All data reported are taken for the four-blade fan except one datum point at $C_{L_u} = 0.4$ in figure 9.

Fan C is the same four-blade high-camber fan as fan B but with the difference that one blade was weakened by cutting out part of the spruce and inlaying a balsa insert. The cut-out was necessary to weaken the blade in order to obtain flutter over a wide range of C_{L_u}. The flutter speeds of fan C refer only to the flutter of the weakened blade. Cutting and inlaying the blade warped the blade sufficiently to give it about 11-percent camber. The value of $C_{L_{u_I}}$ for this section is therefore not the same as that given in table I for the 9-percent-camber Clark YM airfoil section.

Results

Comparative measurements were made with the six-blade fan A and the four-blade fan B to determine the flutter characteristics, maximum power loading, maximum lift coefficient, and efficiency of the two fans. The power loading is expressed in terms of horsepower per square foot. Each blade has an area of about 1/4 square foot.

The results of these tests are given in figures 10(a) to 10(e). The efficiency is defined as the useful power divided by the motor output as measured by a strain-gage dynamometer. The power is the integral of $dQ\,\Delta p$, where Q is the quantity rate of air flow through the fan and Δp is the pressure rise through the fan. The absolute values of these measurements are not very good, but the same systematic errors apply to both fans; consequently, the efficiencies should be useful only for comparison purposes. The fan losses are due to the drag of the airfoil sections and the rotational energy loss. Since the airfoil sections were small and rough (maximum Reynolds number of 1,000,000), the section drag losses were probably higher than for full-scale fans. From the consideration of efficiency, there seems to be little choice between the two fans.

The lift coefficients are given for the 0.9 radius. The lift coefficients are obtained from total-pressure measurements taken behind the fans and by use of equation (6). The rotational-velocity interference factor a' is low for the tip section of the fans tested. This factor was therefore neglected in the determination of W for the calculation of the lift coefficient ($a' = 0$).

Since the model Reynolds numbers were small and the models were rough, the maximum lift coefficients are probably less than would be obtained with larger Reynolds numbers and smoother models. Fan A, having a conventional Clark Y airfoil section, gave maximum lift coefficients of 0.8 at the 0.9 radius and of 0.9 on some of the inboard sections. Fan B, having the 9-percent-camber Clark YM airfoil sections, gave maximum lift coefficients of about 1.0 at the 0.9 radius and of 1.4 at some of the inboard sections. Although the higher-camber fan does give somewhat higher maximum lifts, these high lifts are obtained at some losses in efficiency. The prediction of how much lift would be carried by fans operating at high Reynolds numbers, without separation of flow occurring with a resulting loss of efficiency, is difficult because of some uncertainty of the effect of Reynolds number on the maximum lift.

The blade-tip twisting as a function of the lift coefficient for constant fan speed is given for fan B in figure 11. The lift

coefficient is given for the 0.9 radius and is calculated from total pressure measurements as previously discussed. The twist at the tip was observed by means of a stroboscope and was measured with a protractor on a telescope. Figure 11 shows that for constant operating speed the blade twisting deformation increases the angle of attack at the high lift coefficients and decreases the angle of attack at the low lift coefficients. Note that a lift coefficient exists for which the blade twist is zero. This value of C_L is by definition the experimental lift coefficient of no twist $C_{L_{u_I}}$. The value of $C_{L_{u_I}}$ for fan B is approximately 0.8 (fig. 11). This value is less than the theoretical value, 1.16, for the Clark YM airfoil section given in table I. This discrepancy is believed to be due to section boundary-layer effects. The experimental value of $C_{L_{u_I}}$ for fan A is given in reference 1 as 0.37. Although fan B has an experimental value of $C_{L_{u_I}}$ less than that predicted from theory, the experimental value of $C_{L_{u_I}}$ is about twice that for fan A. A fan with the same section as fan B can be employed at high lift coefficients with a greater margin of safety than can a low-camber fan section.

The decrease of C_L with tip Mach number as shown in figures 10(a) and 10(b) for fan B is obviously caused by the blade twisting and decreasing the angle of attack because the fan is operated at a lift coefficient below the experimentally determined value $C_{L_{u_I}} = 0.8$. The decrease of C_L at high Mach numbers shown for fan B in figure 10(c) is primarily a compressibility effect augmented by the blade twisting in a negative direction because the center of pressure has moved back at the high Mach numbers. Figures 10(d) and 10(e) give results for both fans partly stalled with resulting low efficiency.

The power loading of the fans as given in figure 10 is expressed in terms of horsepower per square foot. The maximum values obtained in these tests are much below those shown in figures 2 and 5 which give theoretical values calculated on a basis of a 45° helix angle and the critical Mach number of an isolated section. For a fan of which the Mach number and helix angle vary greatly with the radius, the maximum values given in figures 2 and 5 cannot be attained. For an axial-flow compressor, however, of which the blades are short and made to operate at essentially a constant helix angle and Mach number, it may be possible to attain a power loading approaching that given in figures 2 and 5.

The critical Mach numbers obtained from figure 4 are given in figure 10. The values of C_L used for obtaining M_{cr} are taken at $M_t = 0.4$. Since C_L changed with tunnel conditions, the critical Mach numbers are different. The critical Mach numbers of both the upper and lower surfaces of fan B are also indicated. For fan B at low lift coefficients a high velocity peak occurs on the lower leading-edge surface; thus, a low critical Mach number results. This localized supersonic region does not seem to have much significance. The conclusion is in agreement with the conclusion in reference 4, which states that the Mach numbers at which large changes in airfoil characteristics occur are difficult to predict especially when sharp pressure peaks exist at the leading edge. In figure 10(b) no significant changes in the lift coefficient or the efficiency are seen to occur until the critical speed on the upper surface has been exceeded. This drop in efficiency is probably due to flow separation caused by shock, as pointed out in reference 7. These tests indicate that the critical speed of the upper surface as calculated by two-dimensional theory is essentially a limiting speed for efficient operation of ducted fans.

One of the most significant results of the investigation is given in figure 9. This figure gives the maximum power absorbed in terms of horsepower per square foot for fans A and B as a function of the lift coefficient C_{L_u} at 0.9 radius. The curve for fan A represents the power absorbed as limited by flutter. The maximum power loading is about 100 horsepower per square foot of blade area and occurs at a value of C_{L_u} of about 0.47. This result is in fair agreement with the theory which shows that the maximum power loading should occur at $C_{L_{u_I}}$ of about 0.37 for fan A. Fan B did not flutter at values of C_{L_u} between 0.5 to 0.85; consequently, this part of the curve is shown as a short-dash line. In this range the power is limited by the maximum speed of the motor. This maximum power loading for fan B is beyond the limits of efficient operation because the fan is operating in the supercritical speed region. The flutter points were obtained at values of C_{L_u} of 0.4, 0.88, and 0.92 and this part of the curve is shown as a solid line. The long-dash curve gives the power loading at the point where the fan efficiency has dropped to 80 percent. The power loading of fan B reaches a maximum value of 150 horsepower per square foot which is considerably greater than that reached for fan A.

The flutter point for fan B at $C_{L_u} = 0.4$ was obtained with a six-blade fan; the points at $C_{L_u} = 0.88$ and $C_{L_u} = 0.91$ were obtained with the four-blade fan B. The steep slope of the power-loading curve for fan B at the high and low lift coefficients

indicates that a fan having high-camber sections can be used successfully to absorb a large amount of power over a certain range of high lift coefficients but that such blades have undesirable flutter characteristics at the low lift coefficients.

The vibration frequencies and flutter speeds are given in table II. The flutter speeds are calculated by the method of reference 1 when the 0.8-radius station is used as the reference station. The maximum and minimum measured flutter speeds are also tabulated. The minimum speeds are those obtained with the blades completely stalled.

The maximum flutter speed for fan A is somewhat less than the calculated classical-flutter speed corrected for compressibility. Fan C checks the calculations quite closely. Fan B had some incipient flutter at a tip Mach number of 0.67 when operating with the tunnel open. This Mach number corresponds to the approximate critical Mach number of the upper blade surface for tunnel-open condition. As the speed was increased into the supercritical region, this flutter disappeared and the blades operated very smoothly to the top speed of the motor which corresponds to a tip Mach number of 0.86. At these top speeds the blade lost most of the lift near the tip and, also, twisted in a negative direction. Although the ducted fan operated smoothly in the supercritical region at speeds above the classical-flutter speed, it does not necessarily follow that such will be the case for three-dimensional bodies.

The last row of table II gives the minimum measured stall-flutter tip Mach number divided by the calculated classical-flutter tip Mach number $\frac{M_{f_{min}}}{M_{f_{cal}}}$. This number is of particular interest when fans are considered which may be required to operate in the completely stalled condition. No reliable theory is available, unfortunately, for predicting this minimum flutter speed, which varies for different blade-section shapes, blade plan form, blade materials, and so forth. At present any design which is intended to operate in the stalled condition should be tested by overspeed whirl tests.

CONCLUSIONS

The results of the analysis and of tests made of two wind-tunnel-fan models to determine the effect of flutter speed and critical

Mach number on the power loading of the blade sections indicated the following results:

1. In spite of the fact that higher lift coefficients result in lower critical speeds, the power that a blade section absorbs at the critical speed is a maximum at the highest lift coefficient the blade section can develop. This fact applies to idealized sections and to conventional sections operating near the ideal lift.

2. If flutter limits the operating speed, the fan absorbs the maximum power when the blade is designed to operate at the lift coefficient of no twist. When this lift coefficient and the ideal or design lift coefficient are identical, a blade operating close to its ideal lift has a maximum critical speed as well as a maximum flutter speed. Any material deviation from the ideal lift coefficient results in a greatly reduced maximum power loading.

3. The anticipated increase of power loading of the high-camber blade was obtained in the tests. There was little difference in the efficiency between the Clark Y and the high-camber Clark YM fans, but the high-camber blades developed somewhat higher maximum lift coefficients. The high-camber blades, however, were found to have very poor flutter characteristics at the low lift coefficients.

4. The fan efficiency decreased rapidly after the sonic velocity on the upper blade surface of the fan sections was exceeded.

Langley Memorial Aeronautical Laboratory
National Advisory Committee for Aeronautics
Langley Field, Va., April 16, 1947

REFERENCES

1. Theodorsen, Theodore, and Regier, Arthur A.: Effect of the Lift Coefficient on Propeller Flutter. NACA ACR No. L5F30, 1945.

2. Theodorsen, Theodore: Theory of Wing Sections of Arbitrary Shape. NACA Rep. No. 411, 1931.

3. Theodorsen, Theodore, and Naiman, Irven: Pressure Distributions for Representative Airfoils and Related Profiles. NACA TN No. 1016, 1946.

4. Abbott, Ira H., von Doenhoff, Albert E., and Stivers, Louis S., Jr.: Summary of Airfoil Data. NACA ACR No. L5C05, 1945.

5. Theodorsen, Theodore, and Garrick, I. E.: Mechanism of Flutter - A Theoretical and Experimental Investigation of the Flutter Problem. NACA Rep. No. 685, 1940.

6. Theodorsen, Theodore, and Stickle, George W.: Effect of a Trailing-Edge Extension on the Characteristics of a Propeller Section. NACA ACR No. L4I21, 1944.

7. Stack, John: Compressible Flows in Aeronautics. Jour. Aero. Sci., vol. 12, no. 2, April 1945, pp. 127-148.

TABLE I.- COEFFICIENTS AND LOCATION OF CENTER OF GRAVITY FOR AIRFOIL SECTIONS

Airfoil	$C_{m_{c/4}}$	$x_{c.g.}$	C_{L_I}	$C_{L_{u_I}}$
Standard Clark Y	-0.085	0.44	0.50	0.45
Clark YM	-.22	.44	1.29	1.16
NACA 16-1012	-.25	.48	1.00	1.06

TABLE II.- VIBRATION FREQUENCIES AND FLUTTER SPEEDS

Items	Fan A	Fan B	Fan C
First bending frequency, cps	74	84	76
Second bending frequency, cps	246	245	220
First torsion frequency, cps	355	365	287
Calculated classical-flutter or divergence speed at 0.8-radius station, fps	772	795	624
Calculated classical-flutter tip Mach number, $M_{f_{cal}}$	0.86	0.89	0.70
Calculated classical-flutter tip Mach number, corrected for compressibility	0.76	0.78	0.64
Maximum measured flutter tip Mach number, $M_{f_{max}}$	0.71	(a)	0.66
Minimum measured stall-flutter tip Mach number, $M_{f_{min}}$	0.34	0.44	0.28
$\frac{M_{f_{min}}}{M_{f_{cal}}}$	0.40	0.50	0.40

[a]No flutter up to maximum operating speed of tip Mach number 0.86.

NATIONAL ADVISORY
COMMITTEE FOR AERONAUTICS

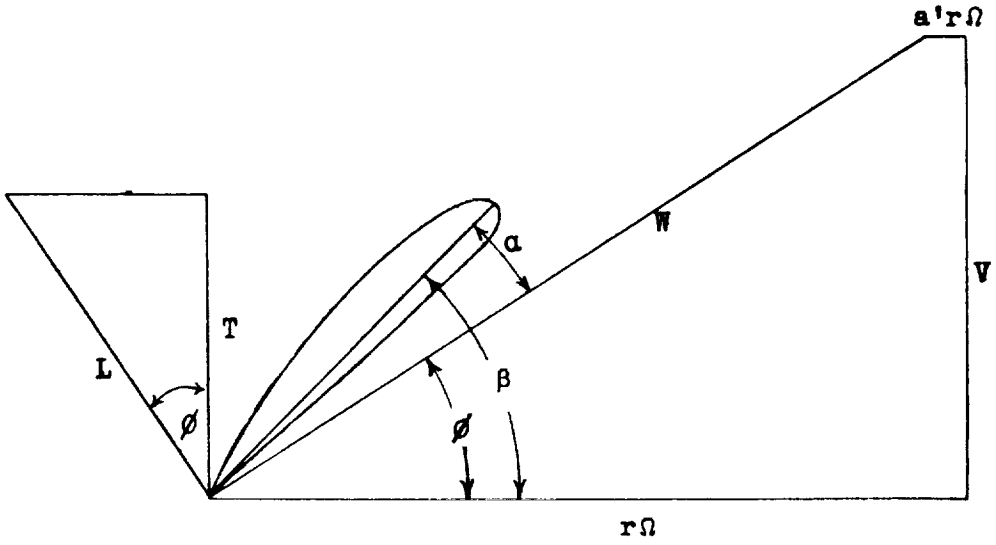

Figure 1.- Diagram of velocities and forces considered in analysis.

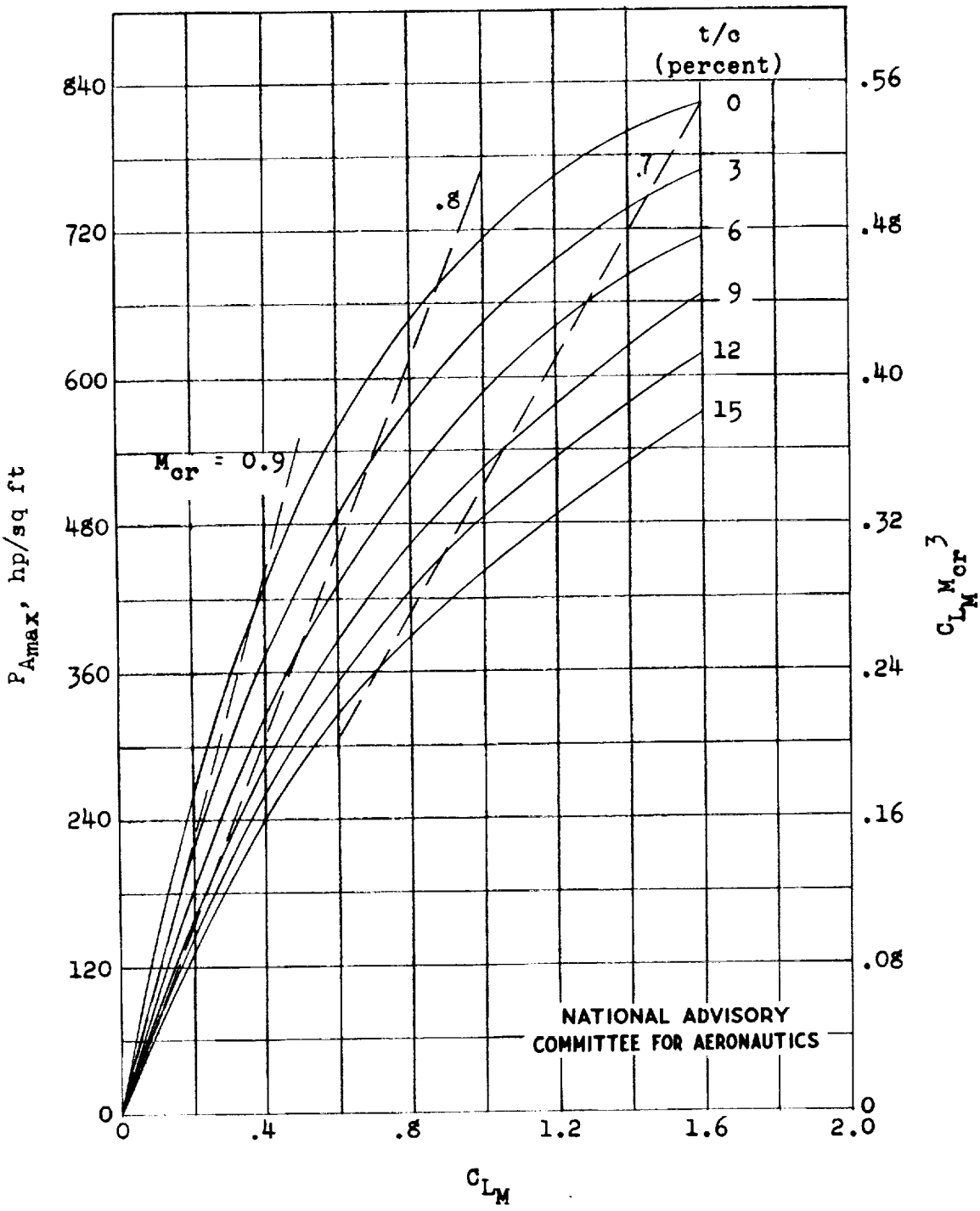

Figure 2.- Maximum theoretical power loading and $C_{L_M} M_{cr}^3$ of idealized airfoil sections for C_{L_M}.

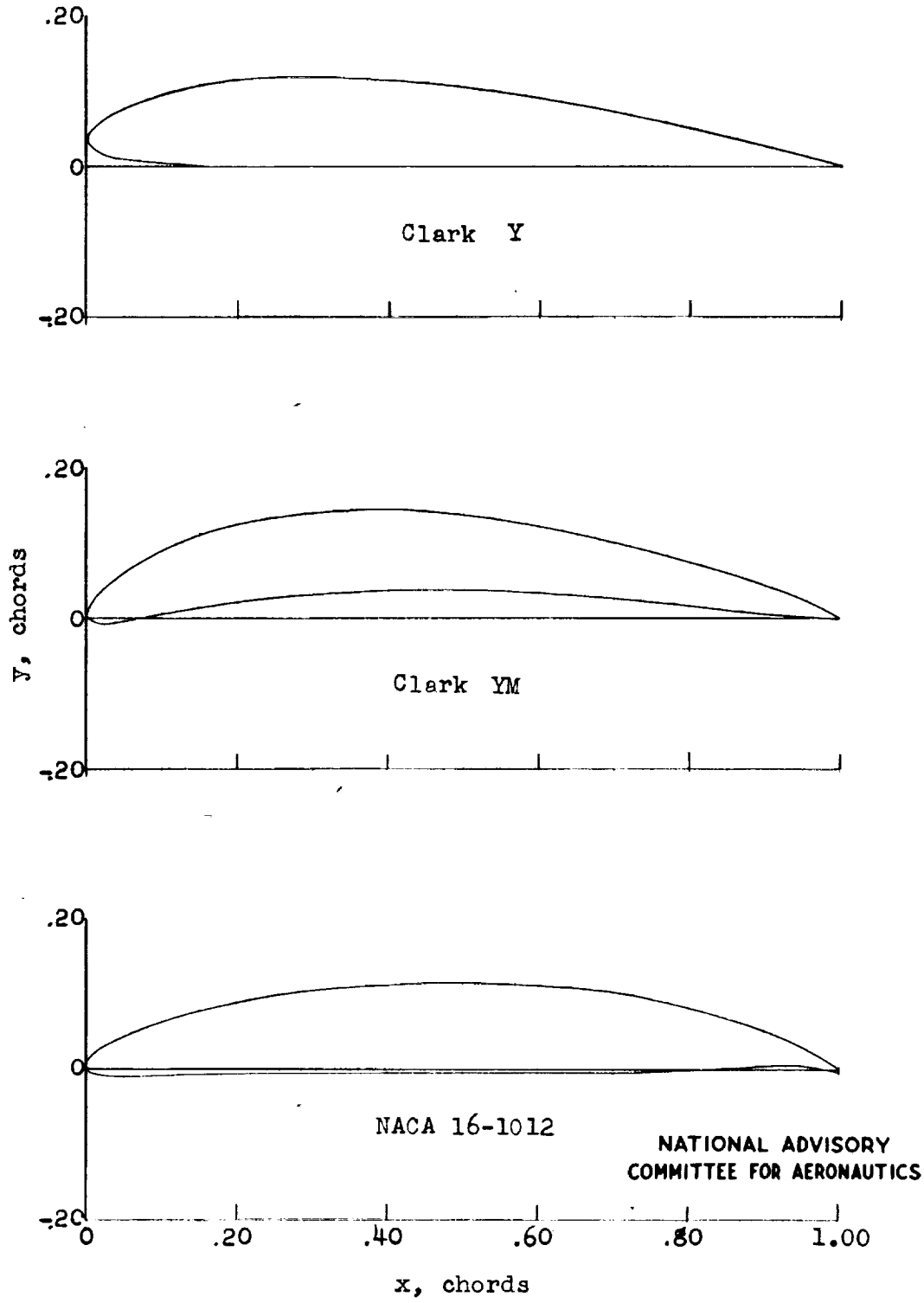

Figure 3.- Shape of airfoil sections.

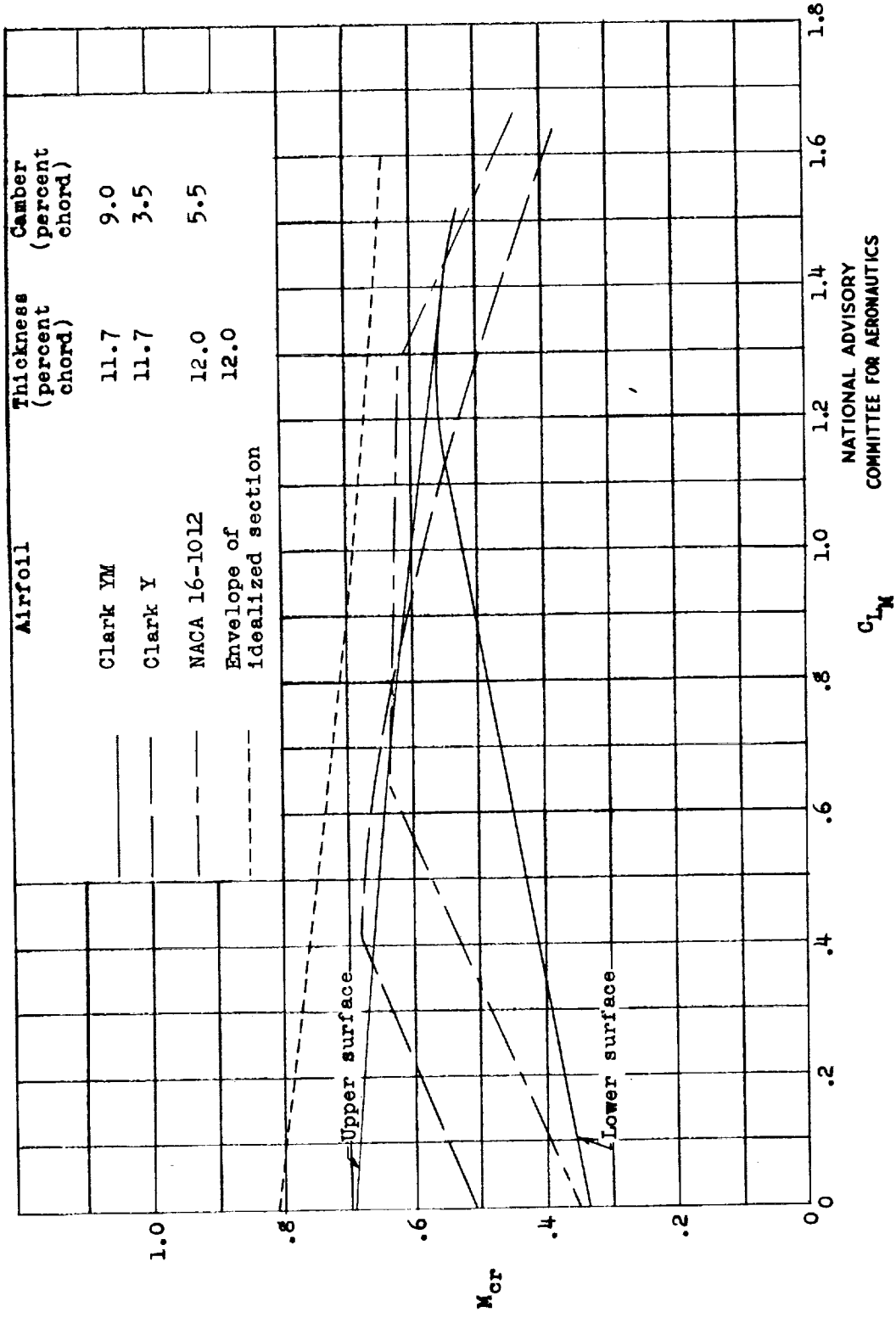

Figure 4.- Comparison of critical Mach numbers of conventional airfoils with idealized airfoil of similar thickness.

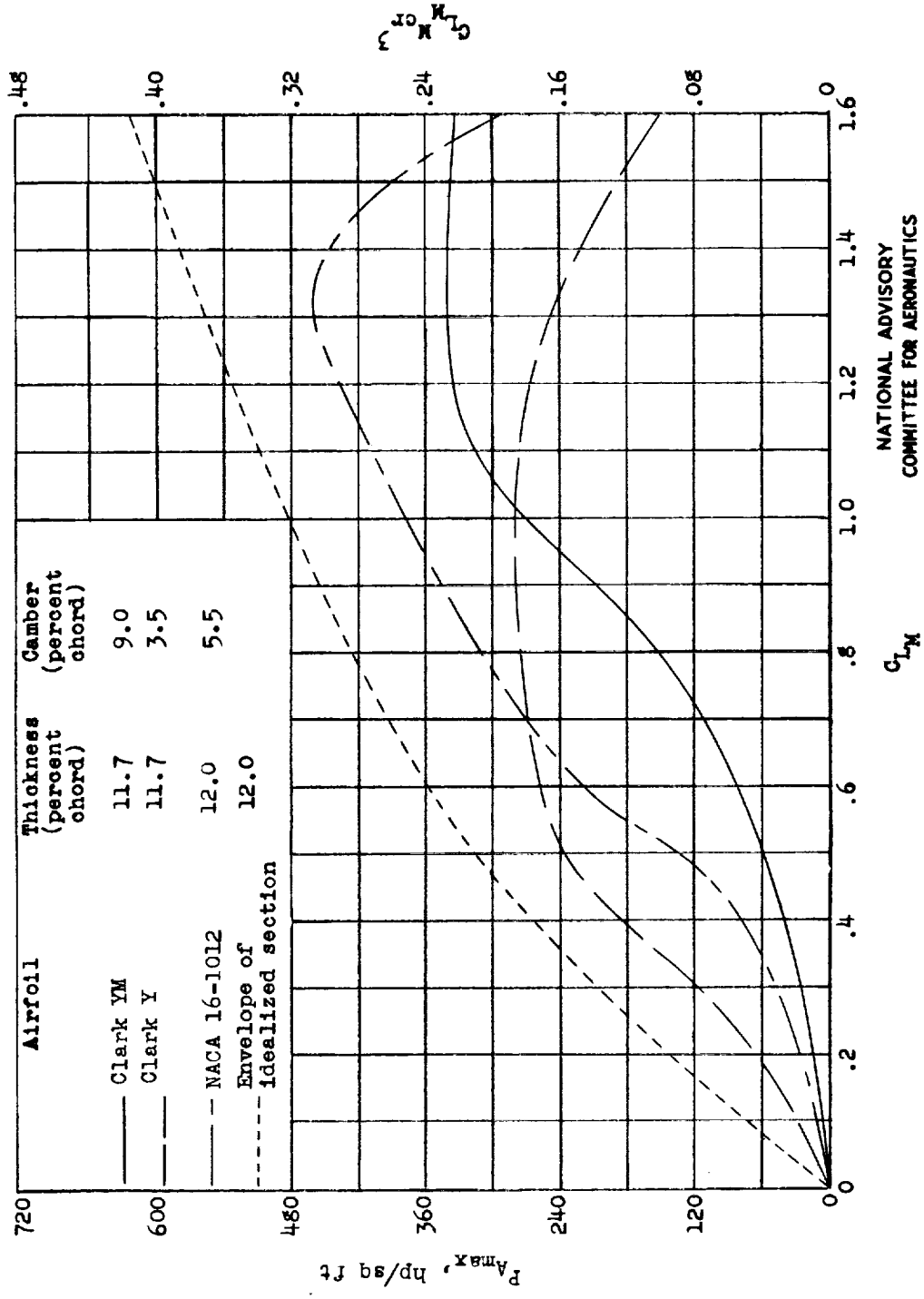

Figure 5.- Comparison of maximum power loading of conventional airfoils with that of idealized airfoil.

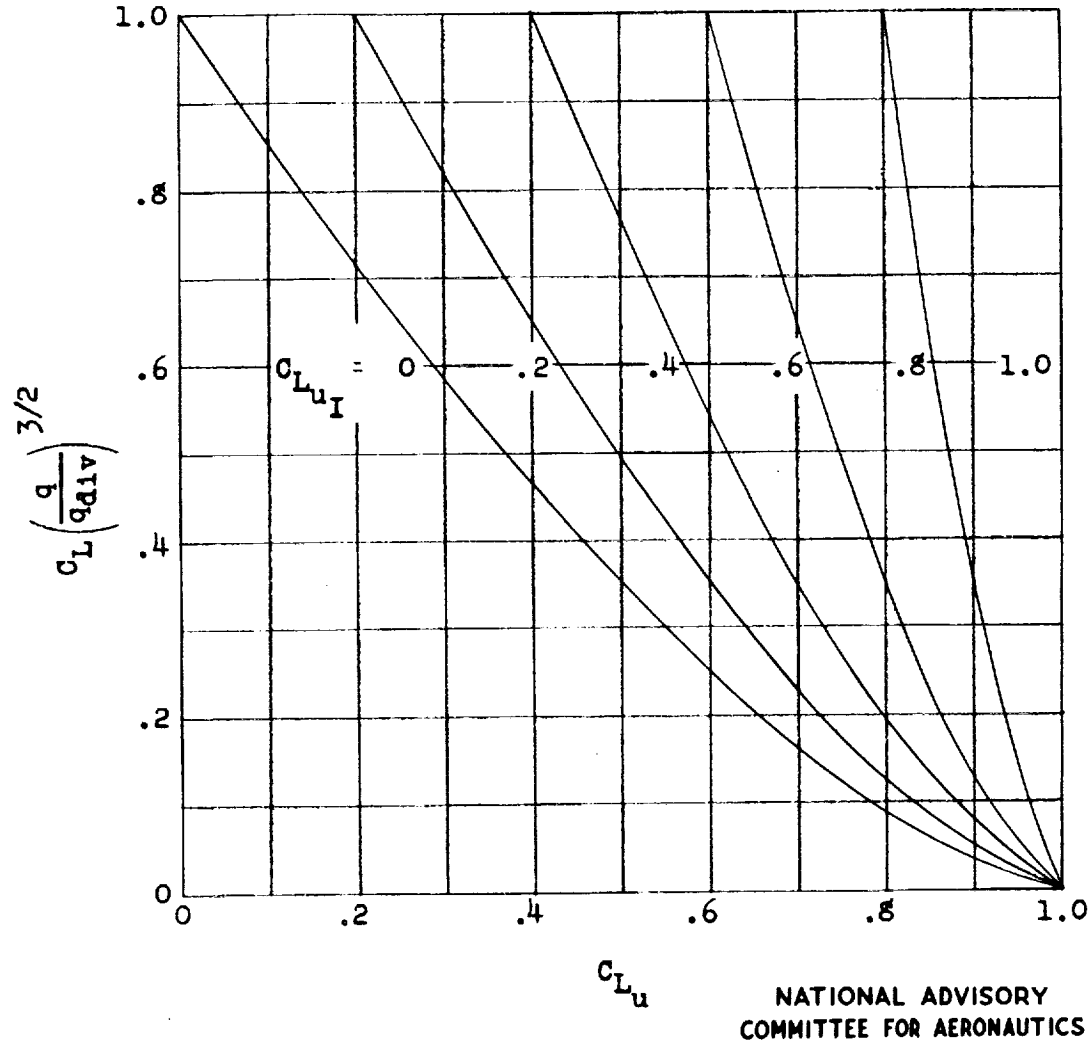

(a) $C_{L_u} > C_{L_{u_I}}$.

Figure 6.- Relative power loading at flutter speed as function of C_{L_u} and $C_{L_{u_I}}$. Flutter assumed at $C_L = 1.0$.

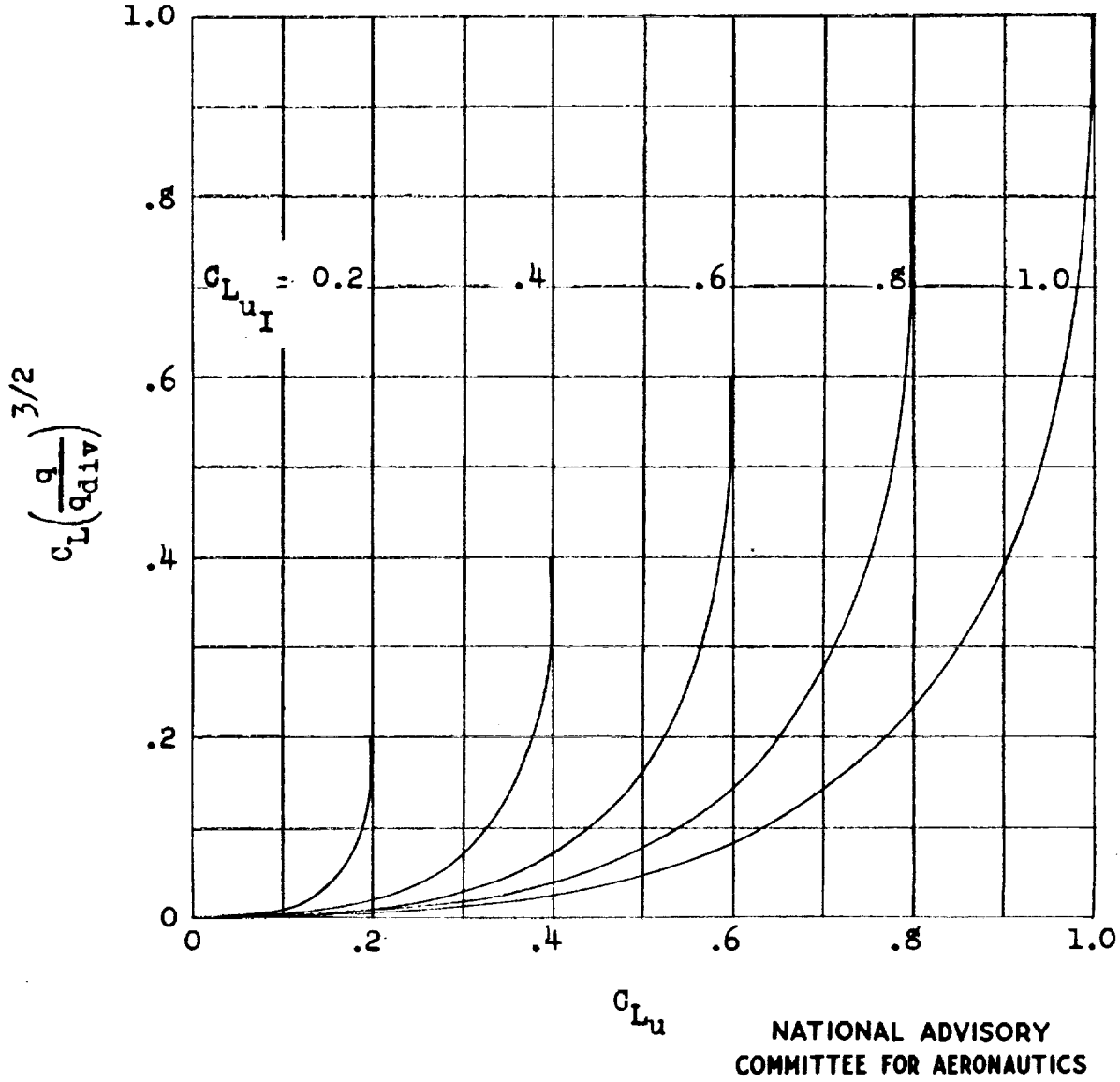

(b) $C_{L_u} < C_{L_{u_I}}$.

Figure 6.- Concluded.

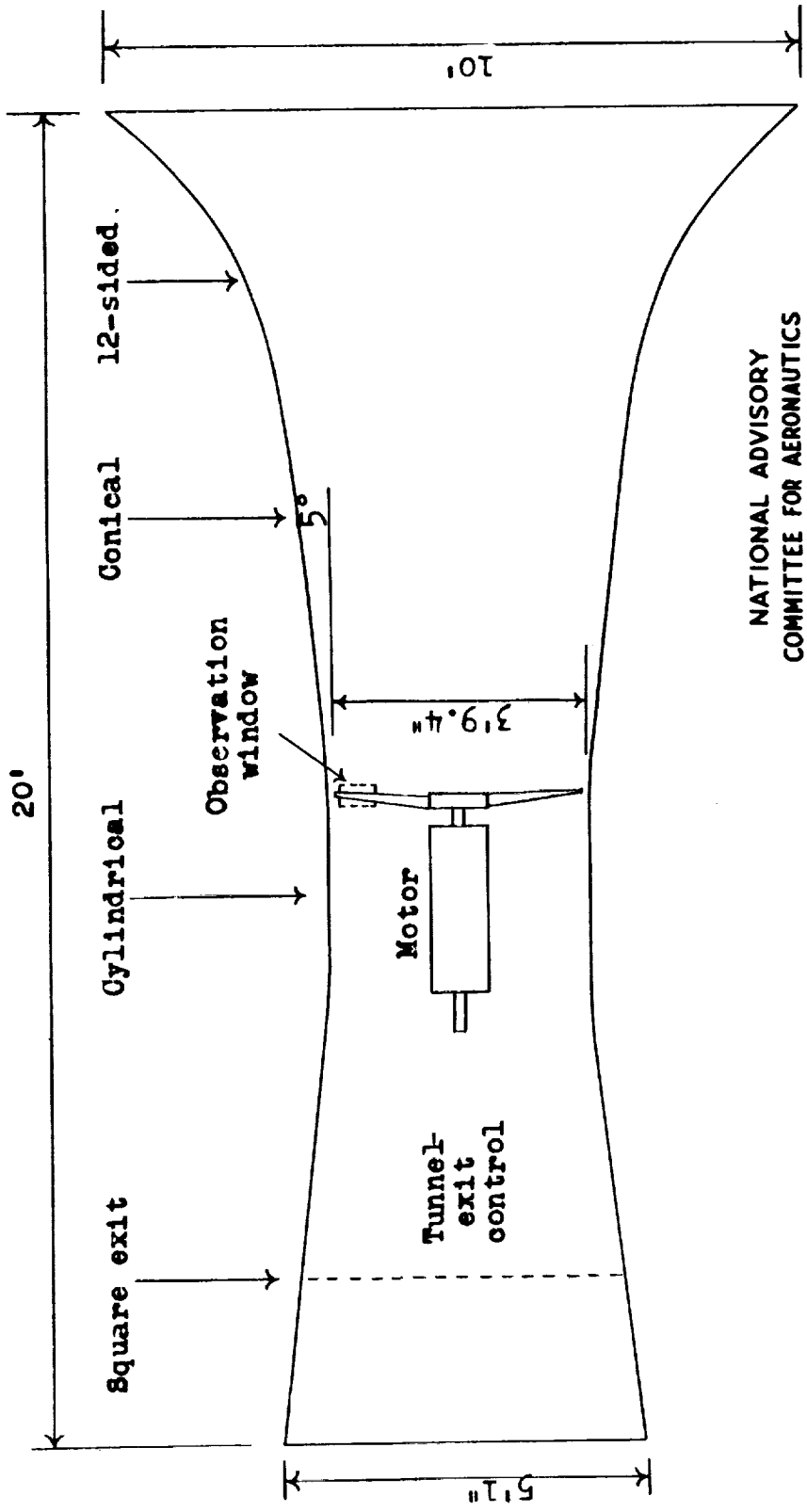

Figure 7.- Cross-sectional view of wind tunnel used for tests (reference 1).

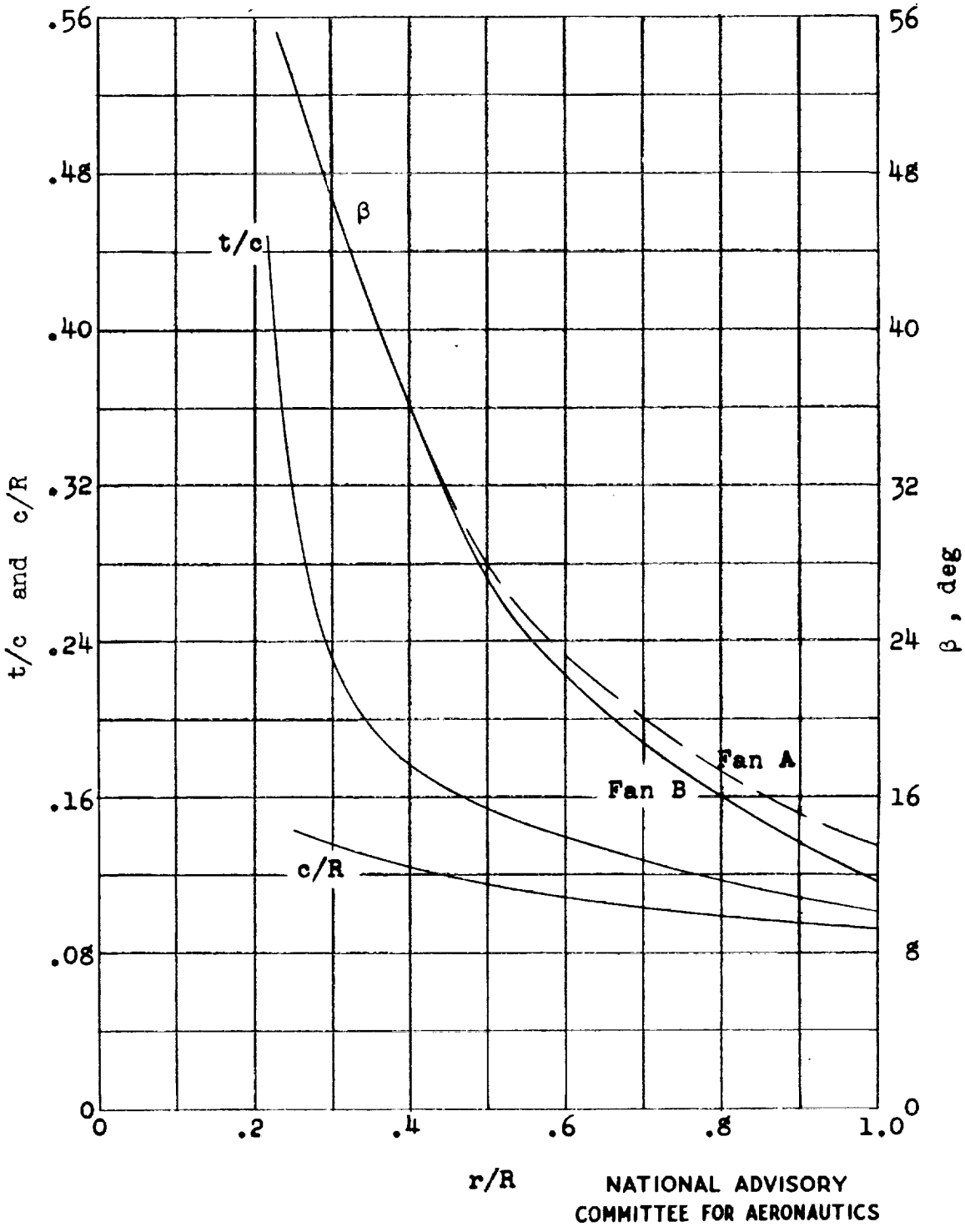

Figure 8.- Blade-form curves.

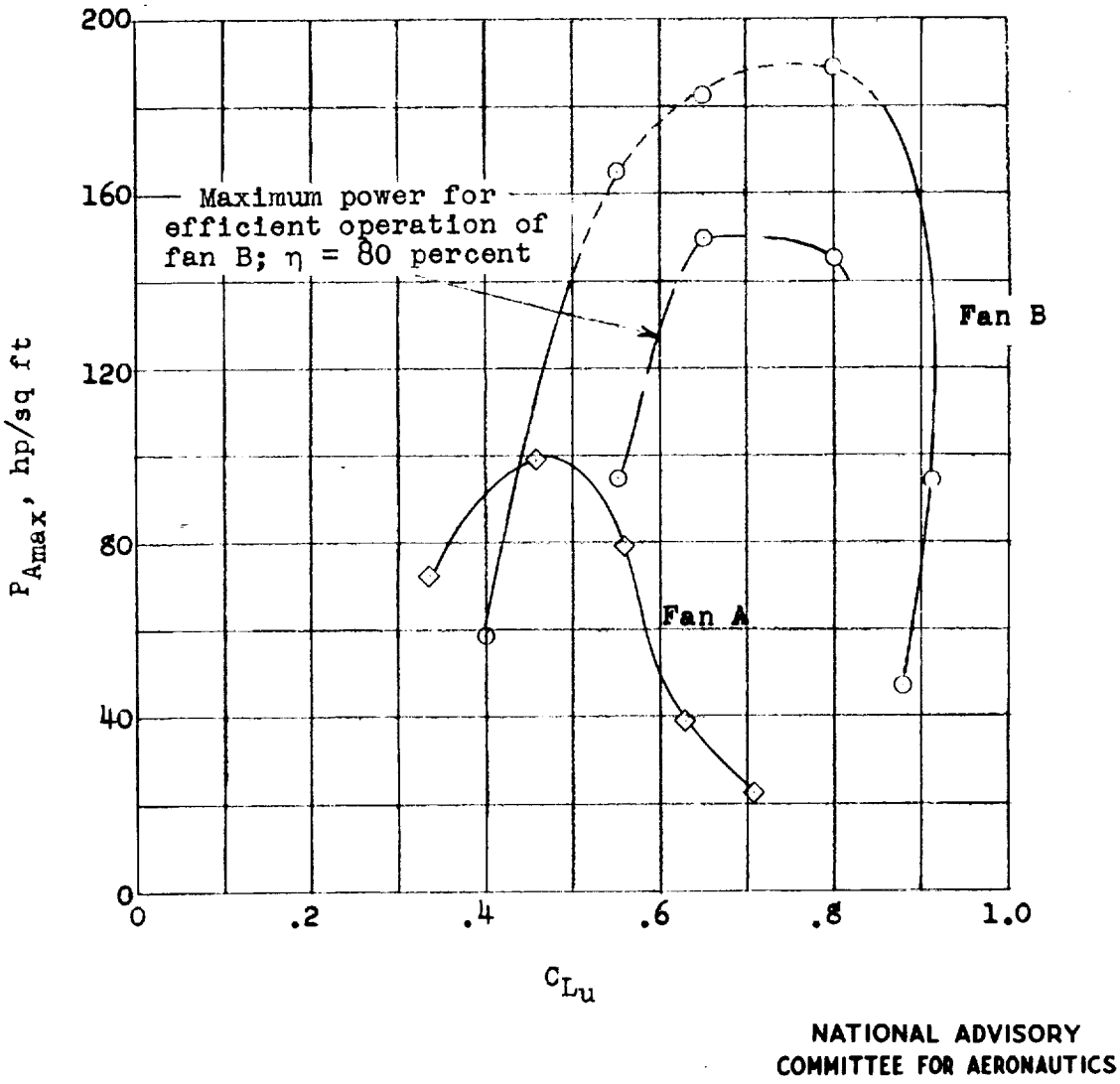

Figure 9.- Maximum measured power loading as function of C_{L_u} at 0.9 radius.

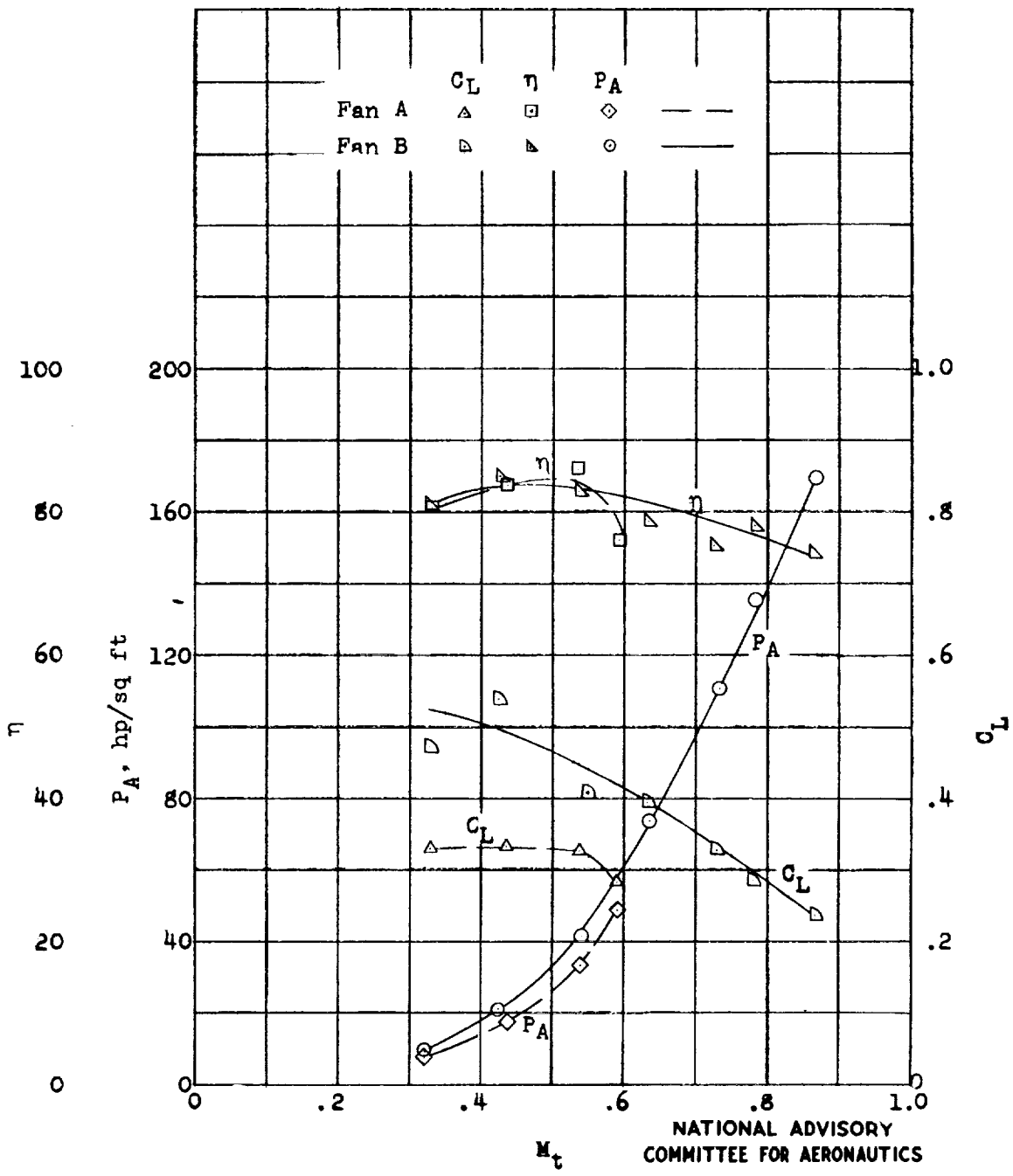

(a) Tunnel open. For fan A, M_{cr} = 0.64; for fan B (upper surface), M_{cr} = 0.65; and for fan C (lower surface), M_{cr} = 0.43.

Figure 10.- Variation of power loading, C_L for 0.9 radius, and fan efficiency with tip Mach number.

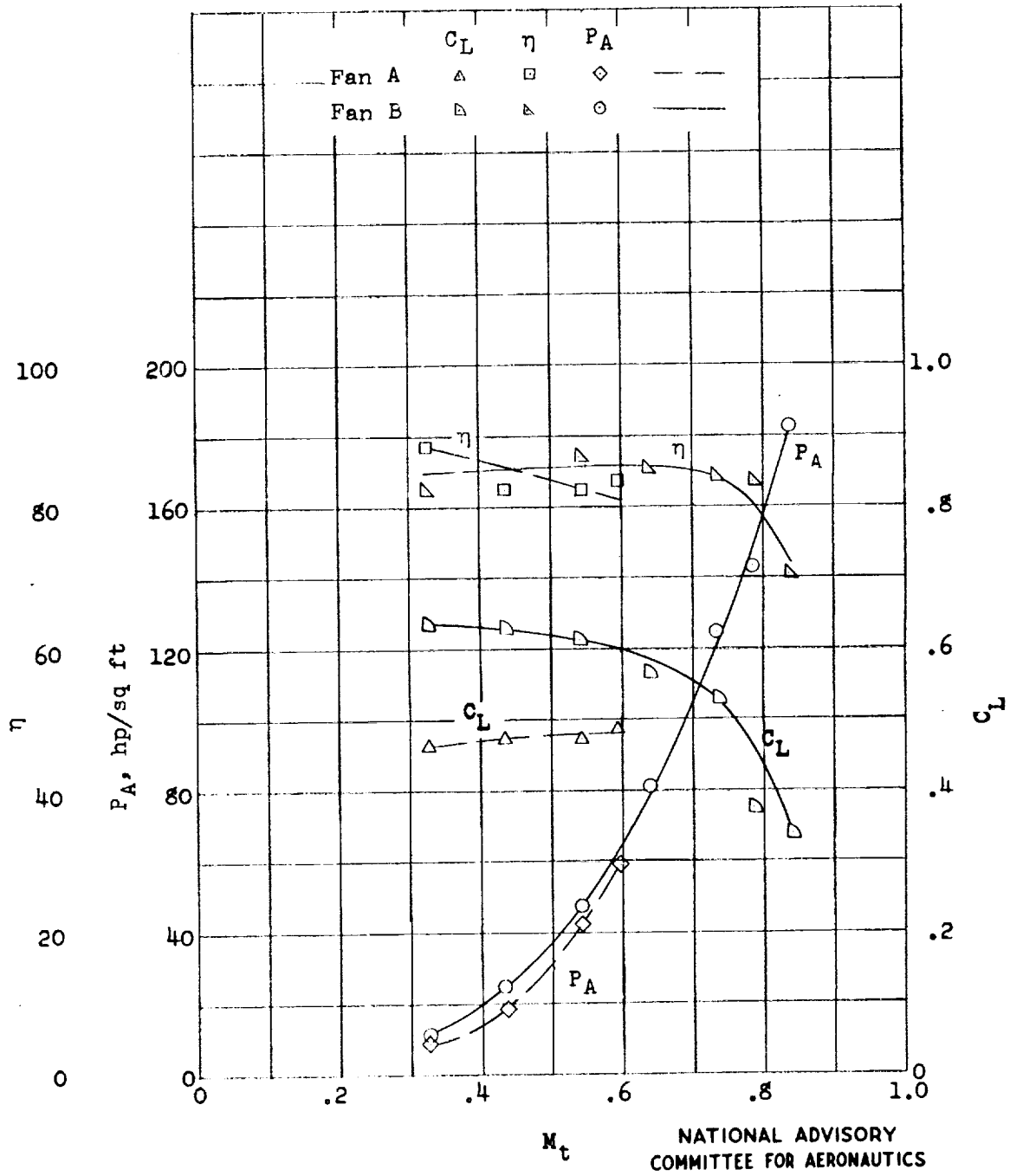

(b) Tunnel blocking, 33 percent. For fan A, M_{cr} = 0.68; for fan B (upper surface), M_{cr} = 0.64; and for fan C (lower surface), M_{cr} = 0.45.

Figure 10.- Continued.

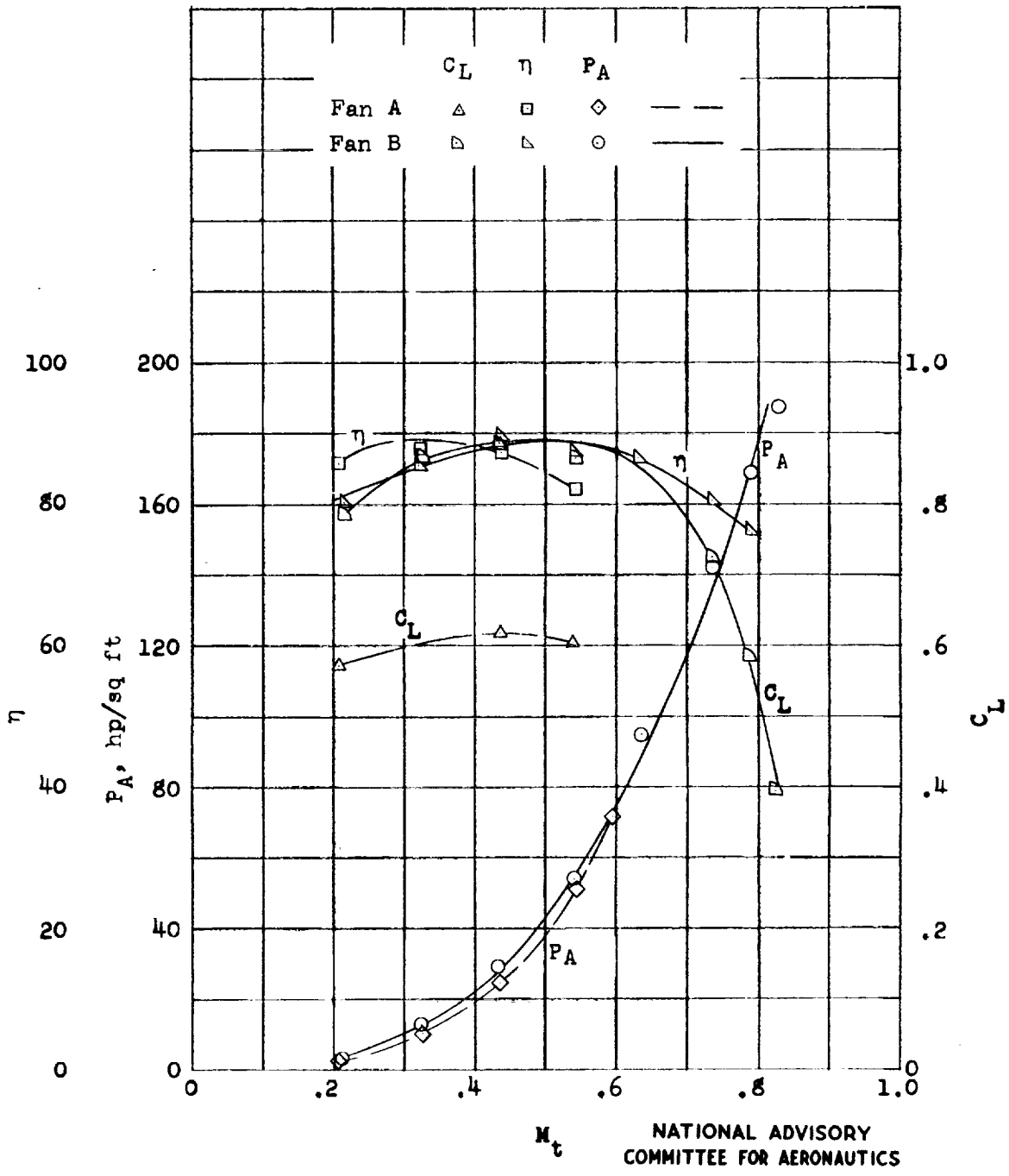

(c) Tunnel blocking, 49 percent. For fan A, M_{cr} = 0.66; for fan B (upper surface), M_{cr} = 0.61; and for fan C (lower surface), M_{cr} = 0.50.

Figure 10.- Continued.

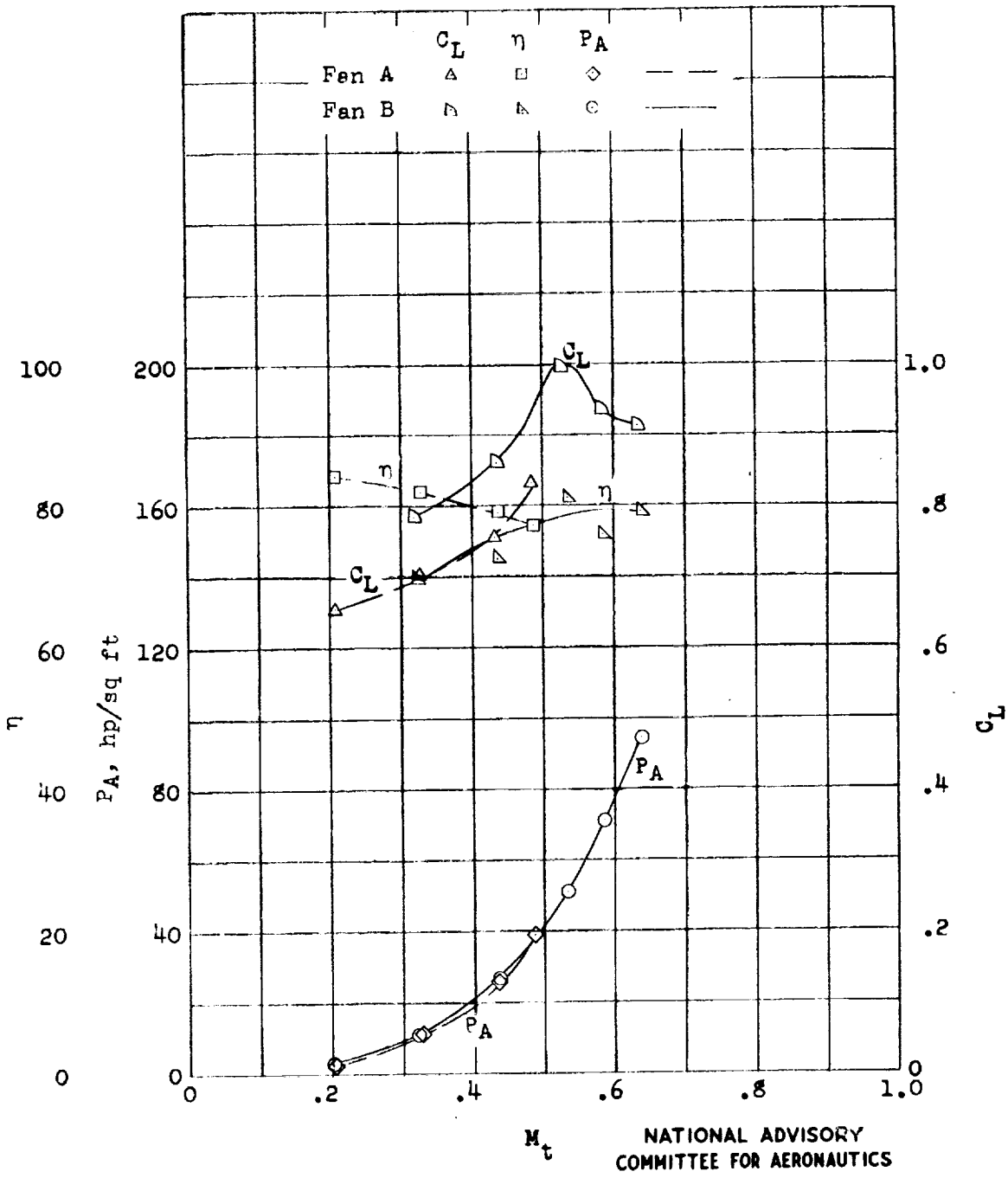

(d) Tunnel blocking, 65 percent. For fan A, $M_{cr} = 0.64$; for fan B (upper surface), $M_{cr} = 0.62$; and for fan C (lower surface), $M_{cr} = 0.49$.

Figure 10.- Continued.

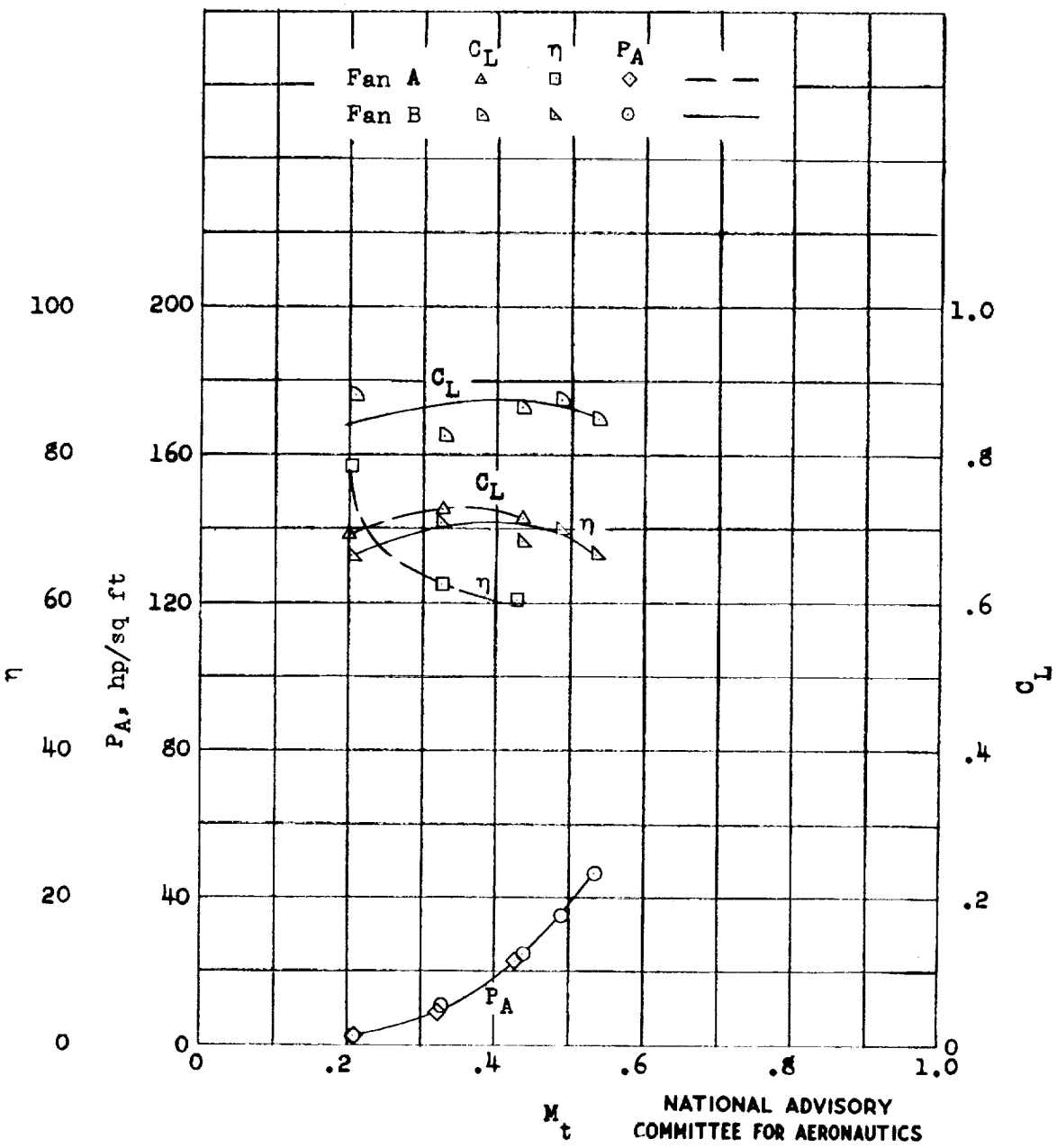

(e) Tunnel blocking, 75 percent.

Figure 10.- Concluded.

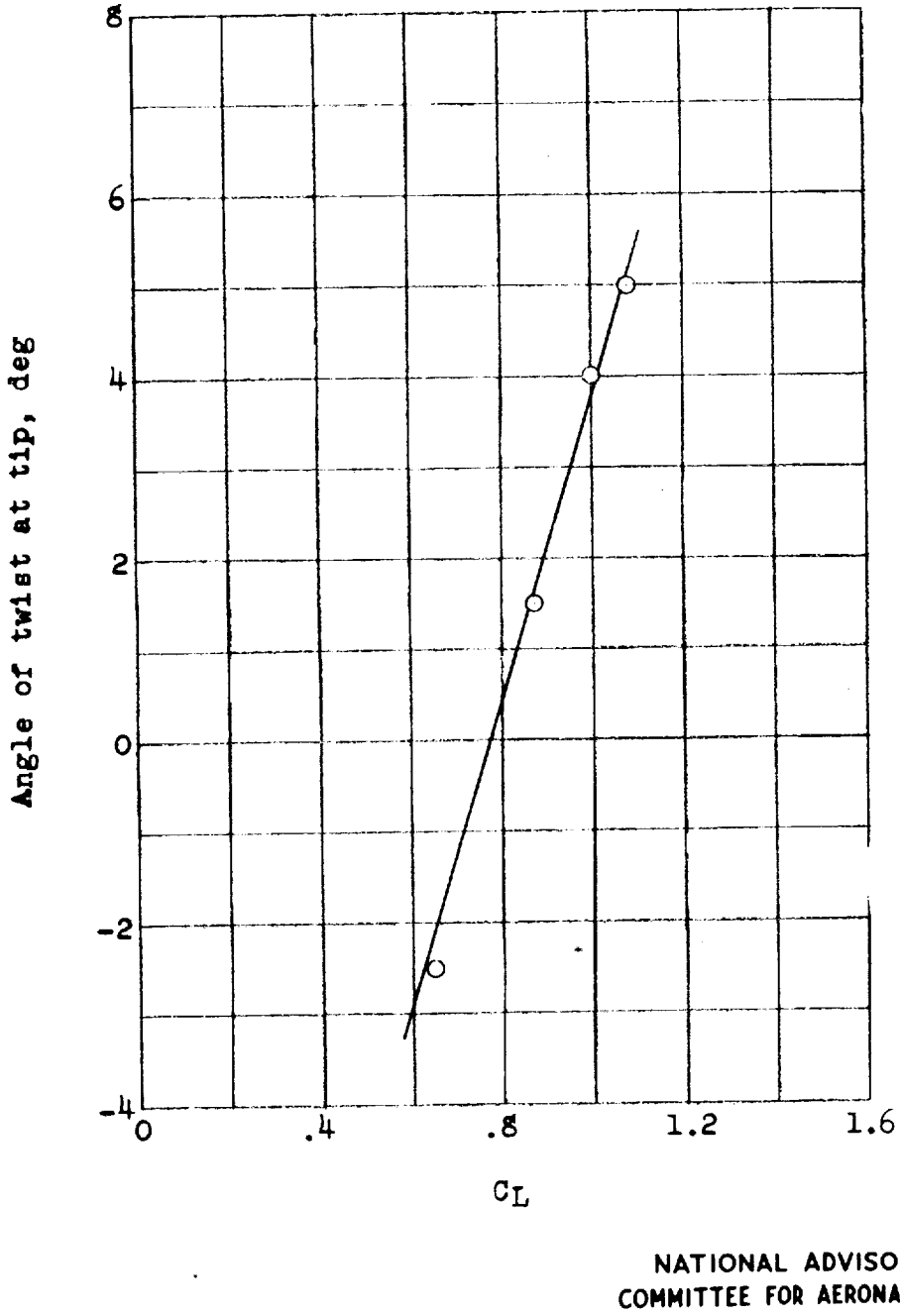

Figure 11.- Blade-tip twisting of fan B as function of C_L at 0.9 radius for constant fan speed; $\frac{q}{q_{div}} = 0.4$.